Multiresolution seismic data fusion with a generalized wavelet-based method to derive subseabed acoustic properties

S. Ker,[1] Y. Le Gonidec[2] and D. Gibert[3]

[1] *IFREMER, Géosciences marines, Centre de Brest, F-29280 Plouzané, France. E-mail: stephan.ker@ifremer.fr*
[2] *Géosciences Rennes (CNRS UMR 6118), Université Rennes 1, Bât. 15 Campus de Beaulieu, F-35042 Rennes cedex, France*
[3] *Institut de Physique du Globe de Paris (CNRS UMR 7154), Sorbonne Paris Cité, 1 rue Jussieu, F-75238 Paris cedex, France*

SUMMARY

In the context of multiscale seismic analysis of complex reflectors, that takes benefit from broad-band frequency range considerations, we perform a wavelet-based method to merge multiresolution seismic sources based on generalized Lévy-alpha stable functions. The frequency bandwidth limitation of individual seismic sources induces distortions in wavelet responses (WRs), and we show that Gaussian fractional derivative functions are optimal wavelets to fully correct for these distortions in the merged frequency range. The efficiency of the method is also based on a new wavelet parametrization, that is the breadth of the wavelet, where the dominant dilation is adapted to the wavelet formalism. As a first demonstration to merge multiresolution seismic sources, we perform the source-correction with the high and very high resolution seismic sources of the SYSIF deep-towed device and we show that both can now be perfectly merged into an equivalent seismic source with a broad-band frequency bandwidth (220–2200 Hz). Taking advantage of this new multiresolution seismic data fusion, the potential of the generalized wavelet-based method allows reconstructing the acoustic impedance profile of the subseabed, based on the inverse wavelet transform properties extended to the source-corrected WR. We highlight that the fusion of seismic sources improves the resolution of the impedance profile and that the density structure of the subseabed can be assessed assuming spatially homogeneous large scale features of the subseabed physical properties.

Key words: Wavelet transform; Wave propagation; Acoustic properties.

1 INTRODUCTION

In the framework of subseabed characterization, seismic imaging is often jointed to ground truth measurements to improve the data interpretation in terms of both morphological structures and physical properties (Pennington 2001; Fomel 2007). Seismic imaging involves low frequency seismic sources (<2 kHz) and requires signal processing, such as deconvolution, to highlight seismic reflectors (Yilmaz 2001). But obviously, a one-to-one relationship between seismic attributes and petrophysical properties (Chopra & Marfurt 2005) is not straightforward (Partyka *et al.* 2000) and highlights the multiscale structure of seismic reflectors, which characterization requires broad-band sources (Widess 1973; Morlet *et al.* 1982; Le Gonidec *et al.* 2002; Le Gonidec & Gibert 2007; Ker *et al.* 2012).

Recent technological improvements of seismic devices such as the deep-towed seismic system SYSIF (Wood *et al.* 2003; Ker *et al.* 2010; Marsset *et al.* 2010) result in a significant extension of the frequency range towards the high frequencies (up to 2200 Hz). The availability of seismic data spanning several octaves in wavelength motivates new methodological developments of signal analysis relying on the multiscale analysis of seismic traces. In this context, the continuous wavelet transform (CWT) naturally appears as a

powerful processing tool (Castagna *et al.* 2003) and in order to consider sound propagation in the analysis, we used the wavelet response (WR) method introduced by Le Gonidec *et al.* (2002). Assuming the validity of the Born approximation (i.e. negligible multiple scattering), both the CWT and WR methods are equivalent and we proposed to extend the use of the ridge functions as a new multiscale seismic attribute (Ker *et al.* 2011), a sparse support of the multiscale information brought by the seismic WR (Mallat & Hwang 1992; Le Gonidec *et al.* 2002). However, the limited frequency bandwidth of seismic sources induce distortions of the ridge functions, as discussed in Ker *et al.* (2012) where we developed a theoretical framework of the source-corrected WR. The method, based on the properties of the Lévy-alpha stable functions, aims at defining a wavelet model for the seismic source with respect to the wavelet formalism, and as a first approach, Gaussian derivative functions with integer derivative orders were considered.

When a single seismic source is involved, the approach is satisfactory and source-corrected multiscale seismic attributes allow characterizing the morphological properties of seismic reflectors (Fig. 1). Note that the characterization is performed in the dilation parametrization of the wavelet formalism, where the relation between dilation and physical properties of the wavelets is not
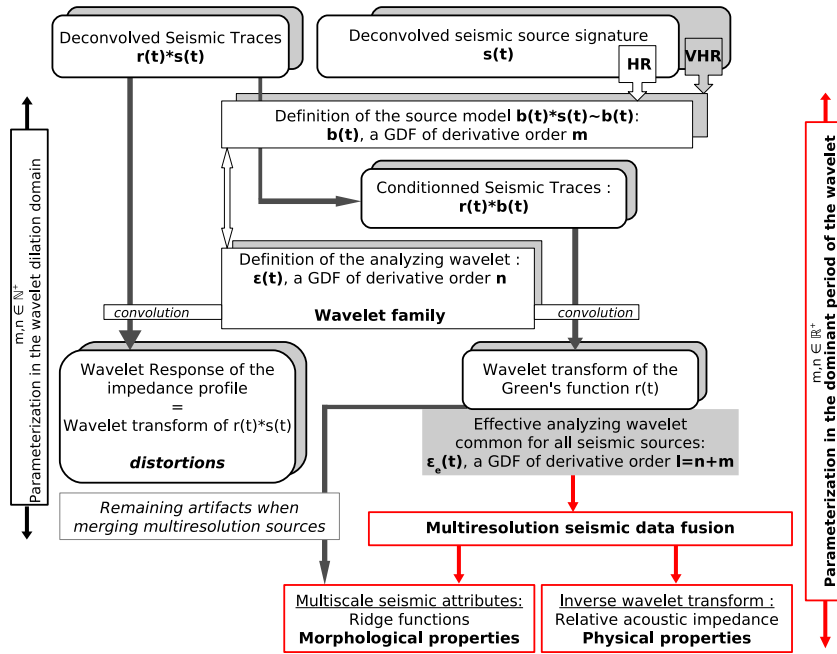
Figure 1. Flow chart of the source-corrected wavelet-based method introduced in Ker *et al.* (2012; GDF, Gaussian derivative functions). In red: the new features proposed in this paper to assess the data fusion from different seismic sources (involving GFDF, i.e. fractional derivative orders: see the text).

straightforward (Ker *et al.* 2012). Moreover, the source-correction suffers from distortions mainly located at large dilations, which limits the method efficiency when merging seismic attributes from multiple sources since artefacts remained in the merged frequency range. Actually, the merged WR that results from the contribution of each seismic source suffered from distortions, located at the junction between individual WRs and the method does not allow working in a continuous source-corrected effective dilation range. As a consequence, methodological developments are necessary to efficiently span the seismic frequency range for multiscale analysis, that is, to perform multiresolution source data fusion (Garguet-Duport *et al.* 1996; Zhou *et al.* 1998; Dong *et al.* 2009). The high resolution and very high resolution seismic sources available with the SYSIF device motivate such new developments and this work fully takes advantage of these multiresolution sources to propose an original approach to both quantify morphological structures of complex reflectors and reconstruct subseabed acoustic properties (Fig. 1).

To make this paper self-consistent, Section 2 recalls the principles of the source-corrected method introduced by Ker *et al.* (2012) and introduce the main definitions of the different terms used throughout the paper. New developments of the wavelet-based method are discussed in Section 3 in order to overcome the limitations encountered in Ker *et al.* (2012). We demonstrate that the optimal Lévy-alpha stable function adapted to the deconvolved seismic source is a Gaussian function and we take advantage of the generalized background of the source-corrected method to develop the method with fractional derivative orders. We also define a new parametrization of the multiscale seismic attributes, based on the breadth of the source model wavelet adapted to the wavelet formalism. Section 4 deals with the optimization of the source model for both high and very high resolution seismic sources, used to perform the source-corrected WR associated to homogeneous thin layers and then to realistic complex subseabed structures. In Section 5, we extend the inverse wavelet transform to the source-corrected WR and we show the capacity of the approach to reconstruct the relative acoustic impedance profile of the subseabed.

2 BACKGROUND OF THE WAVELET-BASED METHOD

In recent works (Ker *et al.* 2011, 2012), we have demonstrated the efficiency of an original wavelet-based approach to characterize multiscale discontinuities of acoustic impedance profiles from seismic data. The method, called the WR introduced by Le Gonidec *et al.* (2002), is a natural extension of the continuous wavelet transform (CWT) where the wavelet family is not convolved with but propagated through the impedance profile $p(z)$ of the medium, that is, the WR is expressed by

$$R\left[\xi, p\right](t, a) \equiv \left(\mathcal{D}_a \xi \otimes p\right)(t) \tag{1a}$$

$$= \mathcal{D}_a \xi(t) * r(t) \tag{1b}$$

$$= W\left[\xi, r\right](t, a), \tag{1c}$$

where $\mathcal{D}_a \xi(t) = a^{-1}\xi(t/a)$ is the dilation operator applied on the analysing mother wavelet ξ, with the dilation factor $a \in \mathbb{R}^+$. The operator $\otimes$ stands for the 1-D propagation and $*$ stands for the convolution operator. Note that the wavelet transform W involves the Green's function of the medium $r(t)$; instead, the WR R involves the impedance $p(z)$, that is, R represents the collection of seismic traces obtained by sounding the medium with a set of wavelet source signals defined by $\mathcal{D}_a \xi(t)$. In Ker *et al.* (2011), we demonstrate that taking into account a real seismic source $s(t)$ with a limited frequency bandwidth, the WR suffers from distortions: $\tilde{R}\left[\xi, p\right](t, a) = W\left[\xi, r * s\right](t, a)$, that is, the WR does not deal with the Green's function of the medium but with the seismic trace $r(t) * s(t)$. In order to recover the wavelet transform properties for the Green's function $r(t)$, we propose a source-corrected method introduced in Ker *et al.* (2012). An overview of the method is depicted in the flow chart of Fig. 1. A wavelet source model $b(t)$ is estimated such that $b(t) * s(t) \simeq b(t)$, defined in the least square sense, where

the deconvolved seismic source signal $s(t)$ is the identity element of the convolution in a limited frequency bandwidth. Considering both the source wavelet $b(t)$ and the mother analysing wavelet $\xi(t)$ as derivatives of a Lévy-alpha stable function $L(t)$ (Voit 2003), that is, $b(t) = \frac{d^m}{dt^m} L(t)$ and $\xi(t) = \frac{d^n}{dt^n} L(t)$ ($m, n \in \mathbb{R}^+$), we show that:

$$\tilde{R}\,[\xi, p]\,(t, a) = [\mathcal{D}_a \xi(t) * b(t)] * r(t) \tag{2a}$$

$$= A \times \mathcal{D}_{a_e} \xi_e(t) * r(t) \tag{2b}$$

$$= A \times W\,[\xi_e, r]\,(t, a_e), \tag{2c}$$

where $\xi_e(t) = \frac{d^l}{dt^l} L(t)$ is the effective mother wavelet with the derivative order $l = m + n$. See Ker *et al.* (2012) for a full description of the effective dilation a_e and the amplitude factor A. As a result, the CWT of a seismic trace $r(t) * s(t)$ can be equivalent to the CWT of the Green's function $r(t)$ of the medium according to the amplitude correction A and a representation following the effective dilation a_e. This result is analogous to the one obtained in the multiscale analysis of potential fields performed with wavelets belonging to the Poisson semi-group (Moreau *et al.* 1997, 1999; Sailhac *et al.* 2009).

3 MERGING SEISMIC SOURCES IN A NEW PARAMETRIZATION

3.1 Previous application on the seismic system SYSIF: limitations and new requirements

In Ker *et al.* (2012), we first applied the wavelet-based method to correct the WR of seismic data acquired by the SYSIF, a deep-towed seismic system developed by Ifremer to image the subseabed (Ker *et al.* 2010; Marsset *et al.* 2010). SYSIF is equipped with two seismic sources covering the high resolution (HR: $220 < f < 1050\,\text{Hz}$) and very high resolution (VHR: $580 < f < 2200\,\text{Hz}$) frequency bands. The SYSIF streamer is a dual channel antenna, where the first channel is a single hydrophone with an offset of 10 m from the seismic source.

As a straightforward application, the wavelet source model was $b(t) = \frac{d^m}{dt^m} e^{-t^2}$, that is, a Gaussian derivative functions (GDF) limited to $m \in \mathbb{N}^+$ as commonly used in seismic imaging (for instance, $m = 2$ is the Ricker wavelet). In this particular context, the minimum derivative order of the analysing mother wavelet $\xi(t)$ was $n = 1$, as required to minimize the complexity of the effective mother wavelet $\xi_e(t)$ (eq. 2c). With an objective of merging different seismic sources, this wavelet $\xi_e(t)$ has to be the same for each source (see Ker *et al.* 2012, for a justification), and we have shown that for the HR and VHR sources of the SYSIF device, the derivative order of $\xi_e(t)$ was $l = 5$, that is, $m = 4$ for both sources.

The first applications of the source-corrected method on both synthetic and field seismic traces demonstrated the potential of the approach, but a lack of efficiency was observed at the transition dilation range between the HR and VHR components. This remaining artefact can be explained by the constraint of both minimizing l in order to reduce the complexity of the multiscale seismic attributes and optimizing the source model. As a consequence, the method limited to $m, n \in \mathbb{N}^+$ does not allow optimizing individual source models and is not fully efficient to perform a source-corrected WR over the whole dilation range composed by several seismic sources. Advanced developments are required in the WR processing to

correctly merge seismic sources, a key point of this paper. Actually, the source-corrected method as recalled in Section 2 can be generalized to $m, n \in \mathbb{R}^+$, and we can take benefit from these fractional derivative orders. The introduction of a fractional order in the source model enables both a better control of the frequency bandwidth of the model spectrum and a reduction of the complexity of the effective analysing wavelet $\xi_e(t)$. This complexity is related to the sum of two derivative orders, n for the mother analysing wavelet $\xi(t)$ and m for the source model $b(t)$. This means that the effective derivative order l of $\xi_e(t)$ for the SYSIF sources should be associated to a low derivative order of the analysing wavelet $n \in\,]0; 1[$ and an optimized source model with $m > 4$.

Furthermore, the method has been developed in Ker *et al.* (2012) with respect to the wavelet formalism, that is, the ridge functions are represented in the dilation domain. In this context, the multiscale seismic attributes depend not only on the reflector topology but also on the effective analysing wavelet, that is, on the derivative order m in particular. To overcome this limitation, which requires a dimensionless proportionality factor between the dimensionless wavelet dilation and the size of the discontinuity, this paper proposes a new parametrization based on the temporal resolution of the source wavelet, that is, based on its dominant period (Gesret *et al.* 2010). For this new approach, we fixed the dilation a_b of the source model $b(t)$ introducing the relation $a_b = 1/(\delta_m B)$, where $1/B$ is the temporal resolution of the seismic source. This is of first importance compare to Ker *et al.* (2012) where a coupling between a_b and m decrease the temporal resolution of the source model when increasing m.

The next two sections address theses new developments applied to the wavelet-based method, required in particular to assess the fusion of different seismic sources. See the flow chart of Fig. 1 to identify the new features and objectives of the generalized method (in red).

3.2 Source model based on optimal Lévy-alpha stable fractional derivative functions

In the general background of the source-corrected method recalled in Section 2, the Lévy-alpha stable function $L(t)$ is not fixed and can be of many kinds, including Lévy, Cauchy and normal distributions, and there is no restriction on the derivative orders m, n, l. We first show that a normal distribution, dealing with Gaussian functions as considered in the wavelet-based method by Ker *et al.* (2012), is actually the optimal distribution to model seismic sources. In a second step, we introduce the fractional derivative orders.

3.2.1 The Gaussian as an optimal Lévy-alpha stable function

In Ker *et al.* (2010), we have shown that the frequency spectrum of a deconvolved seismic source $s(t)$ is characterized by a flat amplitude in a frequency bandwidth limited by a lower frequency and an upper frequency. In the wavelet-based method, $s(t)$ is substituted by a source model $b(t) = \frac{d^m}{dt^m} L(t)$ defined as a Lévy-alpha stable function whose Fourier transform is (Brcich 2005):

$$\hat{L}(f) = \exp\left(- |\pi a_b f|^{\alpha}\right), \tag{3}$$

where the scale parameter a_b is the dilation and $\alpha \in\,]0; 2]$ is the stability parameter of $L(t)$. The spectrum of $\hat{L}(f)$, symmetric about $f = 0$, controls the bandwidth of $b(t)$ which has an infinite frequency support, unlike $s(t)$. This means that the substitution of $s(t)$ by $b(t)$ can not be perfect but is optimal for a frequency spectrum of $b(t)$ included as much as possible in the frequency bandwidth of $s(t)$,

that is, we search for α associated to the Lévy-alpha stable function with the most compact frequency support. A threshold $\gamma > 1$ is required to define a limited bandwidth for $b(t)$: the spectrum of $\hat{L}(f)$ decreases with f, a behaviour that depends on α, and the upper frequency f_{up} is associated to the minimum amplitude $\hat{L}(0)/\gamma$. We can express the limited frequency support $\Delta f = 2f_{up}$ for the source model $b(t)$ by

$$\Delta f = \frac{2}{\pi a_b} \sqrt[\alpha]{\ln \gamma}. \tag{4}$$

Eq. (4) states that for $\ln \gamma > 1$, the bandwidth Δf decreases with α: the most compact frequency support of $b(t)$ corresponds to the stability parameter $\alpha = 2$, that is, we show that a Gaussian function is the Lévy-alpha stable function of the source model $b(t)$ that optimizes the substitution of the seismic source $s(t)$. As a consequence, we consider the Lévy-alpha stable function $L(t) \equiv e^{-t^2}$ in the remaining of the paper.

3.2.2 *Extension to Gaussian fractional derivative functions*

In order to take advantage of the general form of the wavelet-based method, we extend the derivative orders m and n to $\mathbb{R}^+$, that is, without the restriction to $\mathbb{N}^+$ as first applied in Ker *et al.* (2012). Such fractional derivatives are common in physics to model diffusion phenomena in acoustic or electromagnetism through the definition of differentiation operators (Miller & Ross 1993; Kilbas *et al.* 2006). To compute the fractional derivative of the Lévy-alpha stable function, we consider the general property of the Fourier transform (Bracewell 1999)

$$\frac{d^m \hat{L}(f)}{d f^m} = (2i\pi f)^m \hat{L}(f). \tag{5}$$

Thanks to this extension to fractional derivative orders m and n for the source model $b(t)$ and mother analysing $\xi(t)$ wavelets, respectively, the complexity of the former can be balanced by the simplicity of the latter for a fixed derivative order $l = m + n$ of the effective analysing wavelet $\xi_e(t)$. This new development is of first importance in particular when merging different seismic sources, that requires a common $\xi_e(t)$ analysing wavelet, since it allows optimizing each source model independently: each wavelet model is a Gaussian fractional derivative function, noted GFDF in the following.

Note that in the previous paper (Ker *et al.* 2012), the minimum order for the analysing wavelet was $n = 1$ and the source models were defined by $m = 4$, that is, $l = 5$. In order to highlight the capacity of the methodological developments proposed in this paper, we still consider $l = 5$ which gave satisfactory results for the multiscale seismic attributes, but we search for $n \in]0; 1[$ and $m > 4$ in order to optimize each source model and then to improve the source-correction, in particular at the transition dilation range between seismic sources.

3.3 Source model parametrization based on the dominant period

A deconvolved seismic source $s(t)$ with a frequency bandwidth B can be assimilated, as a first approximation, to a Klauder wavelet defined by a width $T_s = 1/B$ which corresponds to the temporal resolution of the seismic source (Gutowski *et al.* 2002). In the wavelet-based method introduced in a previous section, we discussed about the substitution of $s(t)$ by a source model $b(t)$: as a consequence, $b(t)$

has to share the same temporal resolution T_s. The wavelet $b(t)$, defined as a GFDF with a derivative order m, is characterized by a dilation a_b in the wavelet formalism which can be related to T_s by

$$T_s = \delta_m a_b, \tag{6}$$

where the factor δ_m only depends on m. According to the Rayleigh's criterion (Kallweit & Wood 1982), the temporal resolution T_s is given by the dominant period, or breadth, of the wavelet: for instance, the authors defined the dominant period of a Ricker wavelet ($m = 2$) by the trough-trough time. In Ker *et al.* (2012), we extended the definition of the dominant period to any kind of wavelets, that is, not only the Ricker wavelet but also to asymmetrical wavelets defined by odd m values: we define the dominant period as twice the time between two primary extrema of the wavelet. It is important to note that this definition is valid also for a fractional derivative order, that is, for $m \in \mathbb{R}^+$, as illustrated in Fig. 2 for an even ($m = 2$, Ricker wavelet), an odd ($m = 3$) and a Gaussian fractional derivative ($m = 2.5$) functions.
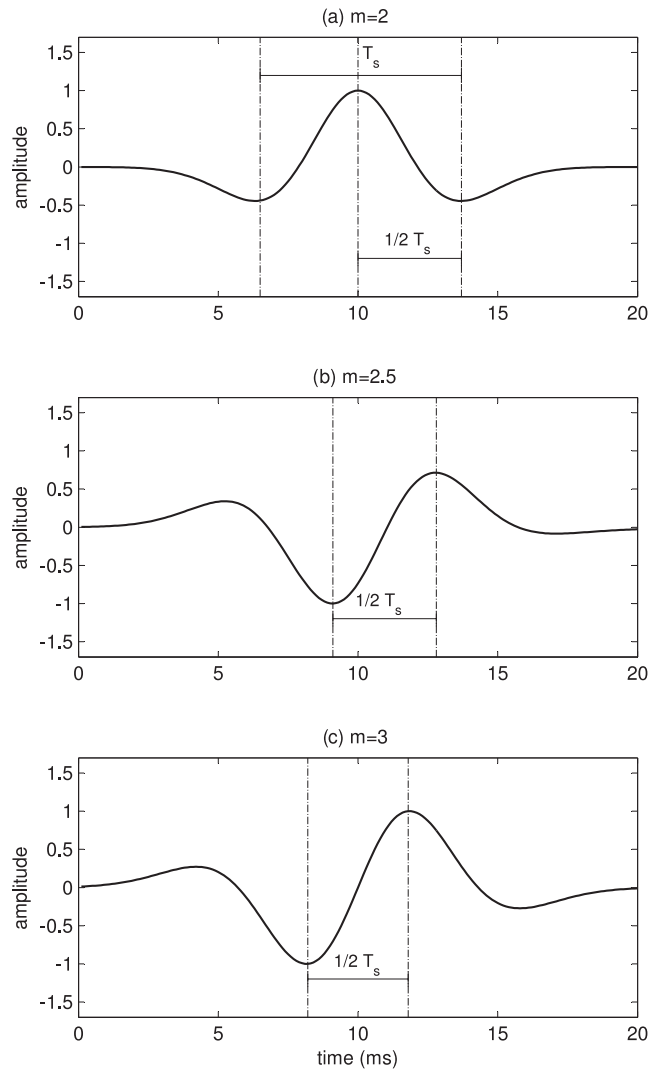
Figure 2. The dominant period T_s, that is, the breadth of the source wavelet, is defined as twice the time between two primary extrema: (a and c) illustrate the case of an even ($m = 2$, the dominant period is also the trough-trough time) and an odd ($m = 3$) Gaussian derivative function (GDF), respectively, and (c) illustrates a Gaussian fractional derivative function (GFDF with $m = 2.5$). Note that all wavelets have the same dominant period.
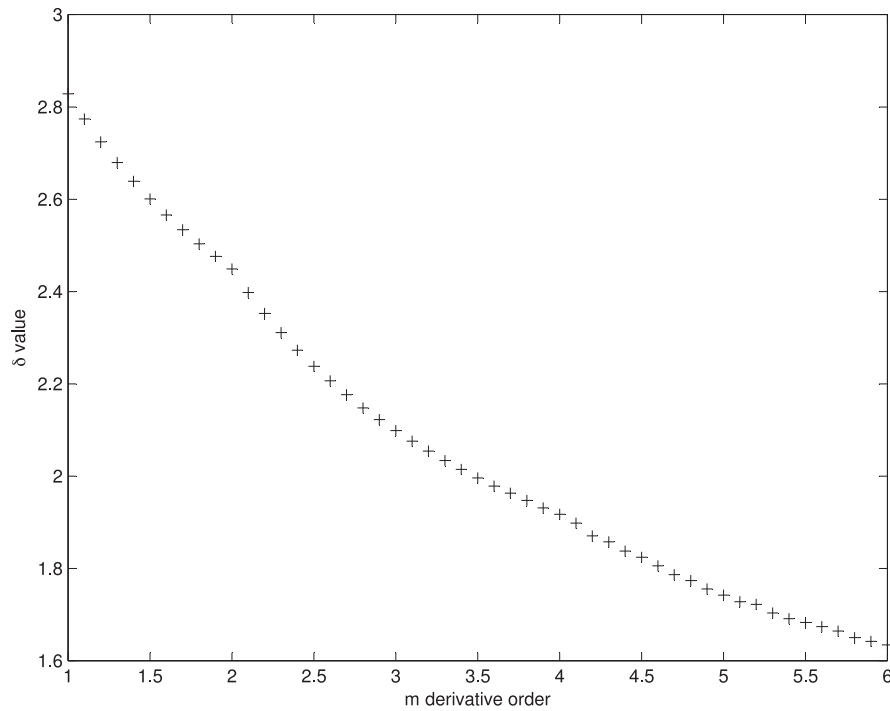
Figure 3. Numerical computation of the δ_m factor as a function of the fractional derivative order m of the GFDF. δ_m enables to relate the dilation a_b of a source model $b(t)$ defined in the wavelet formalism with the temporal resolution of the source $s(t)$.

In most cases, including fractional derivative orders m, numerical computations are required to determine δ_m but analytical expressions exist for $m = 1, 2, 3, 4$ and we can show that $\delta_1 = 2\sqrt{2}$, $\delta_2 = \sqrt{6}$, $\delta_3 = 2\sqrt{(6 - 2\sqrt{6})}$, and $\delta_4 = \sqrt{(10 - 2\sqrt{10})}$. In Fig. 3, we plot δ_m versus the derivative order $m \in \mathbb{R}^+$ up to $m = 6$.

4 WR OF MERGED SYSIF SOURCES: MULTISCALE SEISMIC ATTRIBUTES

In this section, we apply the new methodological results to both the HR and the VHR seismic sources of the SYSIF system so as to obtain a unique wavelet response WR_e in a wide dilation range. We define two GFDF source models, one for each SYSIF source. We also present the effective analysing wavelet $\xi_e(t)$ associated to the merged SYSIF sources: we illustrate the efficiency of the new developments by performing the WR_e of synthetic thin layers. Then, we perform the WR_e of synthetic seismic data: actually based on *in situ* measurements, such data sets allow working with both HR and VHR data at exactly the same subseabed location, which is difficult to perform at sea as the precision in positioning of a deep-towed vehicle is $\approx$20 m in 1700 m water depth.

4.1 Fractional Gaussian derivative models for SYSIF sources

In the wavelet-based method, the criteria to determine the source model wavelet $b(t)$ of a seismic source $s(t)$ is based on both a low wavelet complexity, that is, a low value of the derivative order m and a low quadratic misfit between both sides of $b(t) * s(t) \simeq b(t)$ which is minimized with high values of m. In our previous study (Ker *et al.* 2012), the optimal trade-off was reached for $m = 4$

for each SYSIF sources, associated to a common effective wavelet $\xi_e(t)$ of order $l = 5$ and a maximum misfit of 20 per cent. In this work, GFDF with $m \in \mathbb{R}^+$ allow adapting the model for each SYSIF sources and reduce the misfit to 10 per cent. The following shows that the source-correction with $l = 5$ is fully satisfactory, that is, an optimization of l is not required in this work where we still consider a derivative order $l = 5$ for the effective wavelet $\xi_e(t)$ in order to highlight the comparison of efficiency between the new developments and the initial approach. Note that the morphological structure of a complex reflector is based on multiscale seismic attributes that require l values as lows as possible to reduce the effective wavelet complexity, that is, searching for $l > 5$ is out of interest.

We determine the relative error in $b(t) * s(t) \simeq b(t)$ for different values of the derivative order m in the extended range [1; 6], for both SYSIF sources (Fig. 4a). At low derivatives orders, the efficiency of the substitution strongly decreases, with relative errors larger than 5 per cent. The error stabilizes at $m = 3$ for the HR source and $m = 5$ for the VHR source, with relative errors less than 2 per cent, that is, the range $3 < m < 5$ includes the best GFDF source models for the two SYSIF sources.

According to eq. (1a), the effective wavelet family is related to the analysing wavelet family $\mathcal{D}_a\xi(t)$. As a consequence, we search for the pair of derivative orders n of $\xi(t)$ and m of $b(t)$ which minimizes, in average, the misfit between the effective wavelet family and the reference wavelets, that is, we search for $m = 5 - n$ in the range [3; 5[which minimizes this error (Fig. 4b): $m = 4.6$ ($n = 0.4$) for the VHR source, and $m = 4.9$ ($n = 0.1$) for the HR source. It is important to observe that with fractional derivative orders, we can improve independently the two source models for each SYSIF seismic source while the complexity of the effective analysing wavelet is kept unchanged, that is, the complexities of $b(t)$ and $\xi(t)$ balance.
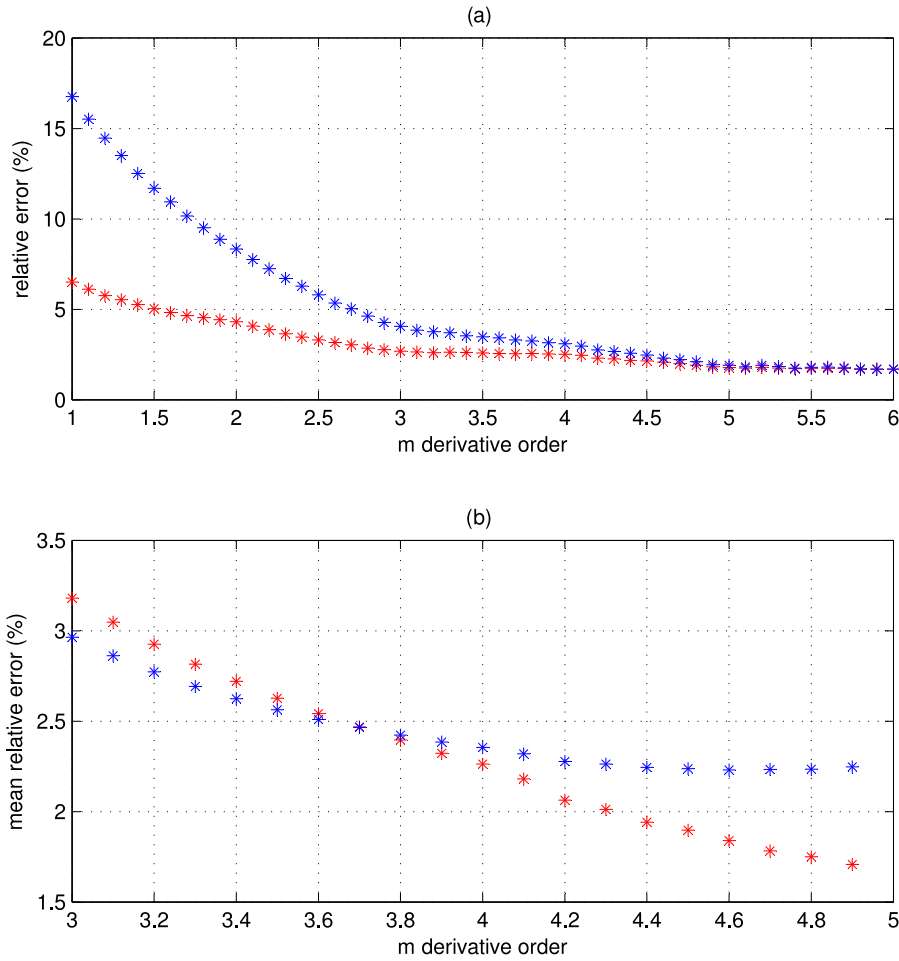
Figure 4. (a) Relative error between $b(t)$ and $b(t) * s(t)$ as a function of the derivative order m: for the HR (red) and VHR (blue) sources of the seismic SYSIF device. (b) Average of the relative errors between the reference wavelets of the fifth derivative order and the effective wavelets $\xi_e(t)$ with the derivative order $l = 5 = m + n$ and $3.9 < m < 4.9$.

4.2 Dominant period of the effective analysing wavelet from merged SYSIF sources

According to the frequency bandwidths B of the HR and VHR sources of the SYSIF device, the dominant periods are $T_{HR} = 1200\,\mu s$ and $T_{VHR} = 620\,\mu s$, respectively. Moreover, the former is associated to the source model $m = 4.9$ and the latter to $m = 4.6$, that is, their factors δ_m are $\delta_{HR} = 1.76$ and $\delta_{VHR} = 1.81$, respectively (Fig. 3). Following eq. (6), it is straightforward to define the associated dilations a_b: 682 and 342 μs, respectively.

Similarly, it is possible to represent the effective analysing wavelet $\xi_e(t)$ versus the dominant dilation a_d instead of the effective dilation a_e as proposed in Ker *et al.* (2012). Actually, a_d corresponds to the dominant period T_d of the effective wavelet and represents the temporal resolution of $\xi_e(t)$

$$a_d \equiv T_d = \delta_l a_e = \delta_l \sqrt{a^2 + a_b^2}, \tag{7}$$

where a, a_b and a_e are the dilations of the analysing, source model and effective wavelets, which derivative orders are m, n and $l = m + n$, respectively. Working with the dilation $\delta_l a_e$ instead of a_e allows considering directly the temporal resolution of the wavelet, that is, a physical more than a geometrical property of the wavelet. Note that the dominant dilation $a_d = \delta_l a_e$ is thus a quantitative parametrization which defines the dilation of the wavelet according to the wavelet formalism.

The dominant dilation a_d depends on the dilation a_b of the source filter, that is, it spans a dilation range that depends on the seismic source frequency content. In the case of the SYSIF seismic sources, this leads to two different dilation ranges, noted $\mathcal{R}_{a_d}^{HR}$ and $\mathcal{R}_{a_d}^{VHR}$ for the HR and VHR components, respectively. The lower bound $a_{d,min}$ of each seismic source dilation range corresponds to the limit $a \to 0$:

$$a_{d,min} = \delta_l a_b = \frac{\delta_l}{\delta_m} T_s. \tag{8}$$

The upper bound is constrained by the lack of low frequency content of $b(t) * s(t)$ which introduces more and more distortions as the dilation increases (see Ker *et al.* 2012), that is, $a_{d,max}$ is defined by a threshold on the mean relative error. When both the HR and VHR contributions are merged, the dominant dilation range of the merged effective wavelets is thus $\mathcal{R}_{a_d} = \mathcal{R}_{a_d}^{HR} \cup \mathcal{R}_{a_d}^{VHR}$ and we define the threshold in order to make $\mathcal{R}_{a_d}$ continuous, that is, to join the upper and lower bounds of $\mathcal{R}_{a_d}^{VHR}$ and $\mathcal{R}_{a_d}^{HR}$, respectively. The lower and upper bounds of $\mathcal{R}_{a_d}$ are then fixed by $a_{d,min}^{VHR}$ and $a_{d,max}^{HR}$, respectively. In this work, we define a threshold of 10 per cent and the dominant dilation ranges for the SYSIF sources are $\mathcal{R}_{a_d}^{VHR} = [620; 1200\,\mu s]$ and $\mathcal{R}_{a_d}^{HR} = [1200; 3260\,\mu s]$. In Fig. 5, we show the relative error of the effective wavelet family in the global range $\mathcal{R}_{a_d} = [620; 3260\,\mu s]$ associated to a virtual broad-band seismic source resulting from the fusion of both sources of the SYSIF
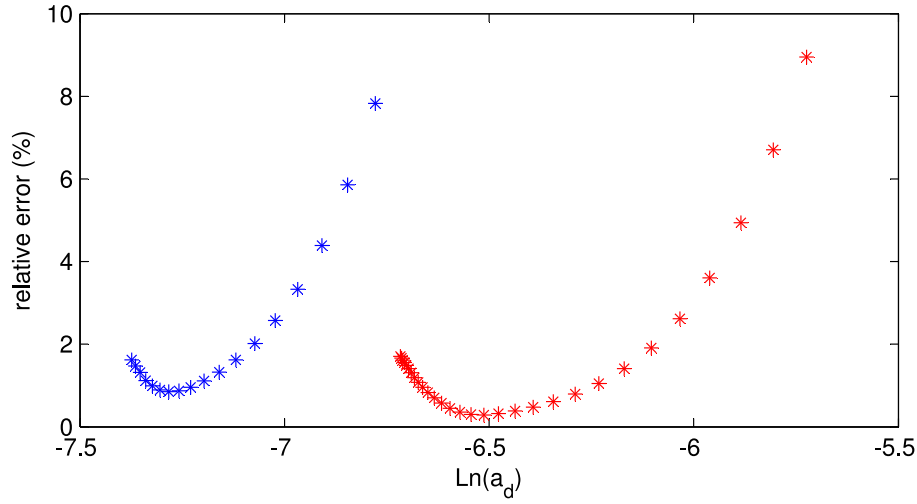
Figure 5. Relative errors between the reference wavelet and the source-corrected analysing wavelet ($l = 5$) as a function of the dominant dilation a_d: for the HR (red) and VHR (blue) sources of the seismic SYSIF device.

device. As expected, the relative error does not exceed 10 per cent in the whole dilation range, and in particular at the transition between the HR and VHR components, which illustrates the efficiency of the new approach based on GFDF.

4.3 Source-corrected multiscale seismic attributes of a homogeneous thin layer

A canonical model to illustrate the source-corrected WR method is a homogeneous layer of thickness Δz sounded by the wavelet family based on $\xi_e(t)$ as defined in the previous section for the SYSIF device. We perform the WR$_e$ associated to the HR and VHR sources for different thickness values $\Delta z = 22, 45$ and 130 cm. The synthetic data set associated to the impedance profile of the layer is based on a forward modelling as described in Ker *et al.* (2011). We extract the multiscale seismic attributes defined by the ridge functions plotted versus the dominant dilation range $a_d \in \mathcal{R}_{a_d}$. The result can be compared to the ridge functions performed with a reference wavelet family without source effects ($a_d \in \mathbb{R}^+$; Figs 6a–c) and the misfit is studied as a relative error in per cent (Figs 6d–f).

For the three thicknesses, the HR and VHR ridge functions are in very good agreement with the reference lines and both components perfectly merged, that is, no discontinuity appears between them (details on the analysis of the ridge functions can be found in Ker *et al.* 2011, 2012). The relative errors are very weak, mainly less than 1 per cent and no more than 3 per cent in the whole dilation range. Since the ridge function is not a linear process, the errors appear lower than the relative errors observed in the effective wavelet family (Fig. 5). Note that in the linear parts of the HR and VHR components, the errors mimic the ones affecting the effective wavelet family.

For the homogeneous layers of thickness $\Delta z = 45$ cm and $\Delta z = 130$ cm, the dominant dilation $a_d^{\max}$ associated to the maximum of the ridge function (Figs 6b and c) is included in the dilation range of the SYSIF device, that is, $a_d^{\max} \in \mathcal{R}_{a_d}$. This means that the maximum is sampled by the SYSIF sources and we can determine the thickness of the layer according to the relation $\Delta z = \lambda/4$ based on the Rayleigh criterion (Kallweit & Wood 1982), where λ is the wavelength associated to the dominant dilation $a_d^{\max}$

$$\Delta z = \frac{a_d^{\max} V_p}{4}, \tag{9}$$

where V_p is the *P*-wave velocity. Note that eq. (9) is valid for all effective wavelets that share the same dominant period range. From Fig. 6(b) for instance, we measure $a_d^{\max} = 1200$ μs which perfectly corresponds to the layer thickness $\Delta z = 45$ cm ($V_p = 1500$ m s^{-1}).

4.4 Source-corrected multiscale seismic attributes of a complex subsurface ground truth data

A more realistic application deals with an *in situ* acoustic impedance profile of a subseabed, which can show complex structures such as multiscale discontinuities (see Fig. 8 discussed in the following section). The seismic source is the SYSIF device used to compute a synthetic data set with the impedance profile obtained from *in situ* and core measurements described in Ker *et al.* (2011). The interest in using such synthetic seismic traces rather than real seismic traces is to sound exactly the same subseabed with both the HR and VHR, which were not experimentally acquired at the same location as a mean distance of ≈ 50 m separates both profiles (Ker *et al.* 2012).

Similarly to the previous section, we perform the effective wavelet response WR$_e$ of the impedance profile with the source-corrected method based on GFDF (with $m = 4.6$ and $n = 0.4$ for the VHR source, and with $m = 4.9$ and $n = 0.1$ for the HR source), and compare the results with the reference WR performed without the source limitation. We also compare the results with the previous method described in Ker *et al.* (2012) and based on GDF with the same derivative order $l = 5$ for both the VHR and HR seismic sources.

The results are plotted in Fig. 7, where the absolute amplitude of the WR performed without source limitation represents the reference WR in the merged dilation range of the HR and VHR seismic sources (Fig. 7a). A strong discontinuity between both source dilation ranges exists in the source-corrected WR$_e$ performed with the previous approach of GDF (HR and VHR: $m = 4, n = 1$), that is, the source merging can not be achieved (Fig. 7b). When applying the new developments based on GFDF (HR $m = 4.9, n = 0.1$; VHR $m = 4.6, n = 0.4$), the source-corrected WR$_e$ is in perfect agreement with the reference WR with fully removed artefacts between HR and VHR components, that is, multiresolution seismic data fusion can clearly be achieved in the merged dilation range (Fig. 7c). A subset of these multiscale seismic attributes also takes advantage of the new method accuracy to characterize morphological structures
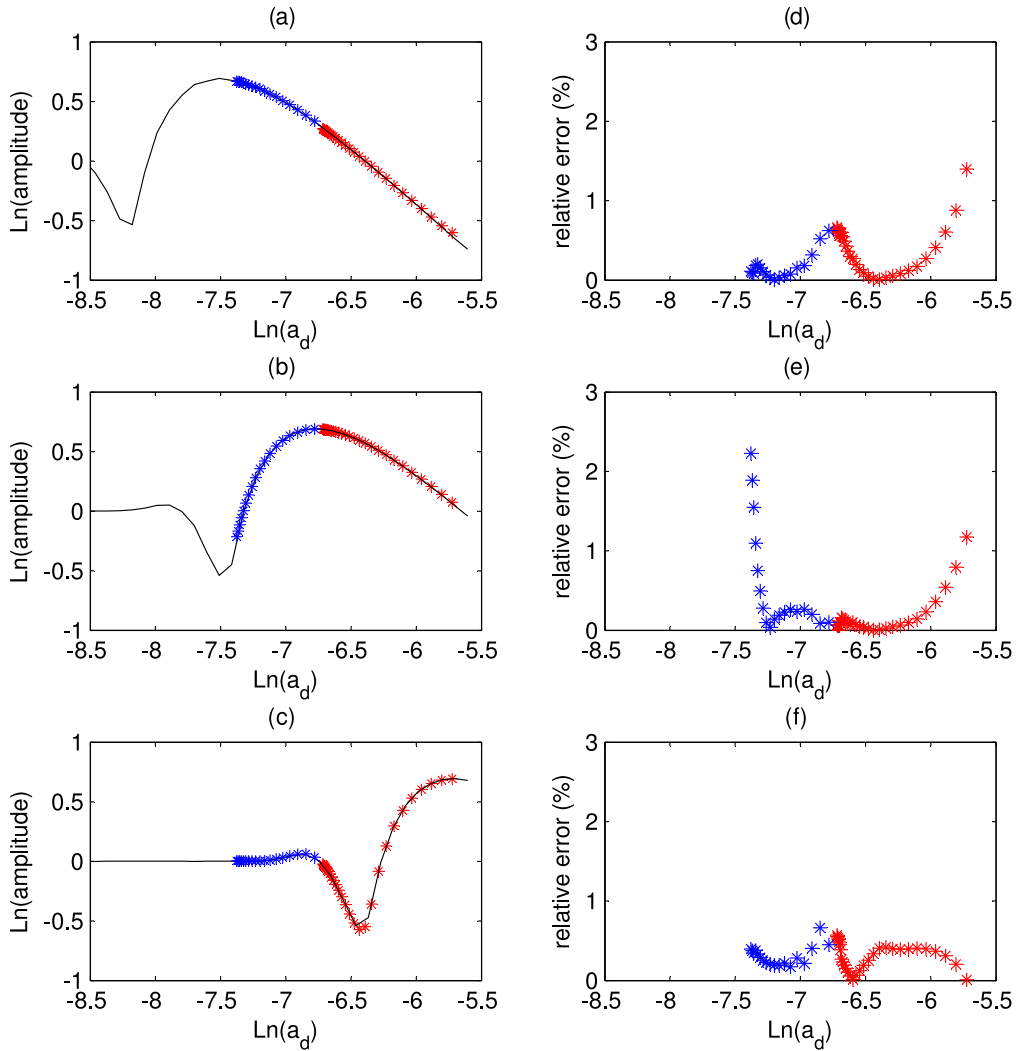
Figure 6. (a–c) Ridge functions extracted from the source-corrected WR_e of homogeneous layers of thicknesses $\Delta z = 22$, 45 and 130 cm, respectively: for the HR (red: $a_d \in \mathcal{R}_{a_d}^{\mathrm{HR}}$) and VHR (blue: $a_d \in \mathcal{R}_{a_d}^{\mathrm{VHR}}$) sources of the seismic SYSIF device. The solid black line stands for the reference ridge function performed with $a_d \in \mathbb{R}^+$. (d–f) Associated relative errors between the source-corrected and reference ridge functions.

of complex seismic reflectors. For instance, the ridge functions of two particular seismic reflectors *A* and *B* (Ker *et al.* 2011, 2012) extracted from the WR_e of Fig. 7(c) are plotted as a function of the dominant dilation a_d (Figs 7d and e) and compared with the reference ridge functions: as expected, the results put in evidence a very good agreement, even at the transition between the HR and VHR components. Thanks to the new parametrization, thicknesses of reflectors *A* and *B* can be directly defined from $\ln(a_d^{\max}) = -6.08$ and $\ln(a_d^{\max}) = -5.9$, respectively: according to eq. (9), $\Delta z^A = 85 \,\mathrm{cm}$ and $\Delta z^B = 100 \,\mathrm{cm}$.

As a conclusion on the new developments proposed in this work, we put in evidence that the source-corrected method based on GFDF in the dominant dilation parametrization allows removing artefacts in the multiscale seismic attributes, and in particular in the determination of morphological structures of complex reflectors. Above all, we show that the method is highly powerful to correctly span the frequency range in the WR multiscale analysis, that is, we are now able to perform multiresolution seismic data fusion by merging different seismic sources. This new approach in seismic topics is promising for future works, as we illustrate in the following with a first application to reconstruct *in situ* high resolution subseabed physical properties.

5 WR OF MERGED SYSIF SOURCES: INVERSE TRANSFORM TO RETRIEVE THE SUBSURFACE IMPEDANCE

The new developments based on both Gaussian fractional derivative functions and a new representation in the dominant dilation domain a_d, are very efficient to merge the WRs of multiple real seismic sources, that is, to span over a large dilation range from. With the equivalence between the WR and the CWT (Le Gonidec *et al.* 2002), the inverse wavelet transform properties can be extended to the source-corrected WR in order to obtain the Green's function of the subsurface.

5.1 Inverse transform of the source-corrected WR

The wavelet transform of a signal $p(z)$ performed with the analysing wavelet $\xi(t)$ is expressed by (Mallat 2008)

$$W\left[\xi, p\right](z, a) = \frac{1}{a} \int_{-\infty}^{\infty} \xi^* \left(\frac{z - \tau}{a}\right) p(z) \,\mathrm{d}z, \qquad (10)$$

where $a > 0$ is the dilation factor and τ is a translational value. From these wavelet coefficients, the signal $p(z)$ can be
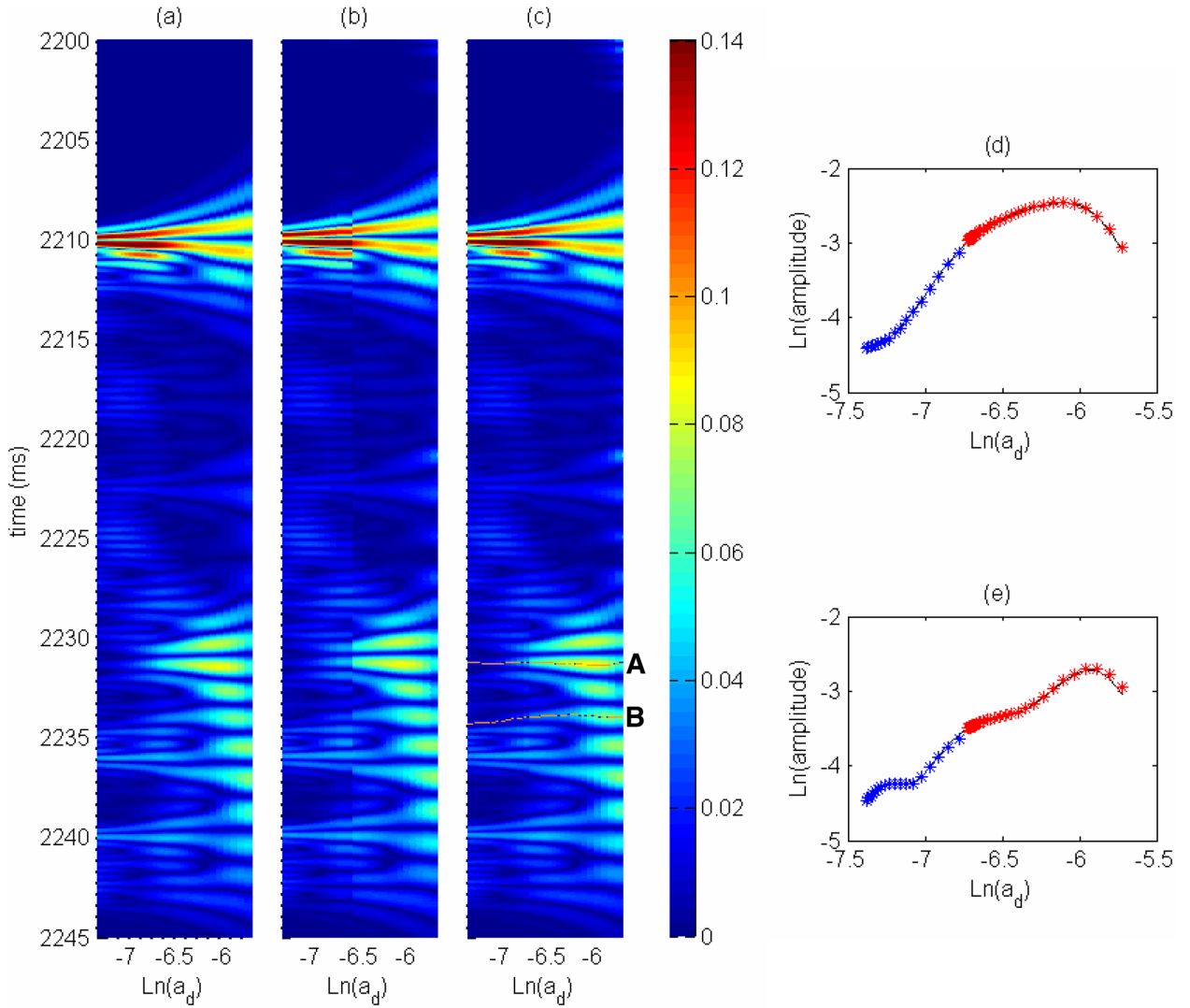
Figure 7. Wavelet responses of the *in situ* impedance log obtained from ground truth measurements with different methods: (a) the reference WR with $a_d \in \mathbb{R}^+$, (b) the previous GDF source-correction method ($m = 4$ for both the HR and VHR sources and $l = 5$) introduced in Ker *et al.* (2012) and (c) the GFDF method developed in this paper ($m = 4.9$ for the HR and $m = 4.6$ for the VHR, and $l = 5$). (d, e) Ridge functions associated to reflectors *A* and *B*, respectively: the HR (red) and VHR (blue) sources of the seismic SYSIF device from the panel (c) and the reference from the panel (a) in solid line.

reconstructed according to the inverse wavelet transform (Mallat 2008)

$$p(z) = \frac{1}{C_\xi} \int_0^\infty \int_{-\infty}^\infty W\left[\xi, p\right](z, a)\, \xi\left(\frac{z - \tau}{a}\right) \frac{\mathrm{d}\tau\, \mathrm{d}a}{a^2}, \qquad (11)$$

C_ξ is a constant associated to the admissibility condition (Mallat 2008): $C_\xi = \int_0^\infty \frac{|\hat{\xi}(\omega)|^2}{|\omega|} \mathrm{d}\omega$, with $\hat{\xi}$ the Fourier transform of ξ.

In the framework of the propagation of plane waves in a non-dispersive 1-D medium and assuming the Born approximation valid, the wavelet response WR is the CWT of the Green's function of the medium (eq. 1c). Thus, it is possible to reconstruct the Green's function $r(t)$ of the medium from the coefficients of the WR (eq. 11):

$$r(t) = \frac{1}{C_\xi} \int_0^\infty \int_{-\infty}^\infty W\left[\xi, r\right](t, a)\, \xi\left(\frac{t - \tau}{a}\right) \frac{\mathrm{d}\tau\, \mathrm{d}a}{a^2} \qquad (12a)$$

$$= \frac{1}{C_\xi} \int_0^\infty \int_{-\infty}^\infty R\left[\xi, p\right](t, a)\, \xi\left(\frac{t - \tau}{a}\right) \frac{\mathrm{d}\tau\, \mathrm{d}a}{a^2}, \qquad (12b)$$

and the impedance profile $p(t)$ can be obtained by integrating the Green's function $r(t)$ over t. Actually, it is a relative impedance profile because the impedance component which contains the mean value of the impedance (i.e. the continuous component) cannot be retrieved.

In order to illustrate the efficiency of this approach, we show here that we can reconstruct the impedance profile of a complex subseabed by using the associated WR coefficients. The impedance profile to retrieve, plotted in Fig. 8(a) versus depth, corresponds to the *in situ* acoustic impedance log determined from ground truth data, already used in Section 4.3 and described in previous works (Ker *et al.* 2011, 2012). When this impedance profile is sounded with a reference wavelet family without any source limitation, we can determine the WR coefficients for a dilation range extended to $a \in \mathbb{R}^+$: using the integration form of eq. (12b), we reconstruct the impedance profile plotted in Fig. 8(b). The high frequency variations are in very good accordance with the initial impedance profile which continuous component has been removed, that is, the reconstructed impedance profile shows positive and negative values (Fig. 8b).
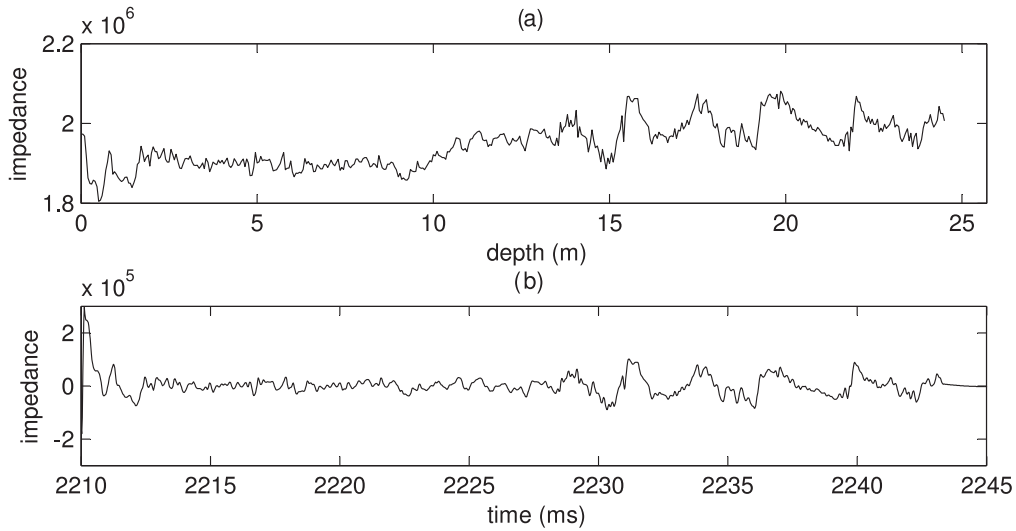
Figure 8. (a) Acoustic impedance profile (unit: Pa.s m^{-1}) obtained from density and sound velocity measurements on ground truth data as a function of depth. (b) Relative acoustic impedance profile reconstructed with the inverse wavelet transform of the reference WR ($a \in \mathbb{R}^+$) as a function of the two way traveltime.

When the WR of the impedance profile involves a seismic source, the dilation range is limited to $a_d \in \mathcal{R}_{a_d}$ according to the WR$_e$ analysis developed in the previous sections: the effect is to partially reconstruct the impedance profile, noted $\tilde{p}(t)$, with the partial Green's function defined by

$$\tilde{r}(t) = \frac{1}{C_{\xi_e}} \int_{\mathcal{R}_{a_d}} \int_t \tilde{R}\left[\xi_e, p\right](t, a_d)\, \xi_e\left(\frac{t-\tau}{a_d}\right) \frac{\mathrm{d}\tau\,\mathrm{d}a_d}{a_d^2}. \qquad (13)$$

According to these new developments, we are able to perform the inverse wavelet transform obtained from both the HR and VHR SYSIF sources used to compute synthetic seismic data for the *in situ* impedance profile plotted in Fig. 8(a). The results are plotted in Figs 9(a) and (b) for the HR and VHR sources, respectively, that is, for $\mathcal{R}_{a_d}^{\mathrm{HR}}$ and $\mathcal{R}_{a_d}^{\mathrm{VHR}}$. Even if both results involve the same initial impedance profile, they differ because of different limited dilation ranges. This highlights the effect of partially reconstructed profiles when a reduced dominant dilation range is involved, that is, the efficiency of the inverse wavelet transform obviously derives some benefit from merged seismic sources. Actually, we show in Fig. 9(c) the result $\tilde{p}(t)$ reconstructed when we merge the HR and VHR components: the result is in very good agreement with the reference inverse transform performed with $a_d \in \mathbb{R}^+$ (Fig. 8b) when no limited frequency bandwidth seismic source is involved. In that case, we increase the dominant dilation range to $\mathcal{R}_{a_d} = \mathcal{R}_{a_d}^{\mathrm{HR}} \cup \mathcal{R}_{a_d}^{\mathrm{VHR}}$, which is continuous thanks to the source-corrected method developed in this work, that is, the reconstruction of the impedance profile is improved when the HR and VHR seismic sources are merged. Note that $\tilde{p}(t)$ is a smooth version of the reference inverse transform (red curve) and clearly puts in evidence the efficiency of the optimal source-corrected method to quantify the main multiscale acoustic contrasts in complex subseabed structures.

It is interesting to discuss about the vertical resolution of the impedance profile. For a seismic source of frequency bandwidth B, the vertical resolution is given by $Vp/2B$ (Gutowski *et al.* 2002), where $Vp \simeq 1485\,\mathrm{m\,s^{-1}}$: the resolutions are 45 and 90 cm for the VHR and HR sources, respectively. When both sources are merged into a virtual broad-band seismic source, the vertical resolution increases to 38 cm: if not accessible directly with the individual seismic data sets, this improved vertical resolution can be expected

in $\tilde{p}(t)$ when the inverse wavelet transform is performed in the merged dominant dilation range $\mathcal{R}_{a_d}^{\mathrm{HR}} \cup \mathcal{R}_{a_d}^{\mathrm{VHR}}$.

5.2 Impedance profiles extracted from seismic SYSIF data

The previous section deals with HR and VHR synthetic seismic traces associated to a common *in situ* acoustic impedance profile which can be reconstructed from the merged source-corrected WR. In this section, we work on field seismic traces acquired by the SYSIF deep-towed seismic system in the close vicinity (110 m) of the location site of the *in situ* acoustic impedance profile: it is important to remember that the HR seismic acquisition, the VHR seismic acquisition and the subseabed samples do not correspond exactly to the same location (the distance between both traces is $\approx$50 m). As shown below, a consequence is a difference between impedance profiles related to *in situ* measurements and seismic data, mainly due to the acquisition conditions rather than the method itself.

Similarly to the previous approach, we perform the source-corrected WR of both the HR and VHR seismic traces and reconstruct the relative impedance profile $\tilde{p}$ from the inverse wavelet transform. Results are plotted in Fig. 10(a) for $a_d \in \mathcal{R}_{a_d}^{\mathrm{HR}}$, in Fig. 10(b) for $a_d \in \mathcal{R}_{a_d}^{\mathrm{VHR}}$ and in Fig. 10(c) for the merged dilation range $a_d \in \mathcal{R}_{a_d}$. In each case, we also plot the impedance profile obtained from the *in situ* measurements in the same dilation range ($\mathcal{R}_{a_d}^{\mathrm{HR}}$, $\mathcal{R}_{a_d}^{\mathrm{VHR}}$ and $\mathcal{R}_{a_d}$). We observe good agreements, in particular in the recovering of the main structures located at $t > 2230$ ms which slight temporal shift is attributed to the difference in the spatial locations of the different data sets. At earlier times, low acoustic impedance contrasts induce low signal-to-noise ratio, that is, we focus the comparison for $t > 2230$ ms. The HR data are more sensitive to the large scale structures, clearly identified with $a_d \in \mathcal{R}_{a_d}^{\mathrm{HR}}$. The small scale features require the higher seismic frequencies of the VHR data. These new results put in evidence the efficiency of the source-corrected method which merges the HR and VHR sources, that is, we are now able to define the relative impedance profile $\tilde{p}(t)$ of the subseabed from broad-band seismic traces acquired with the SYSIF device.

In future works, HR and VHR acquisitions should be performed at the same location in order to improve the combination of the
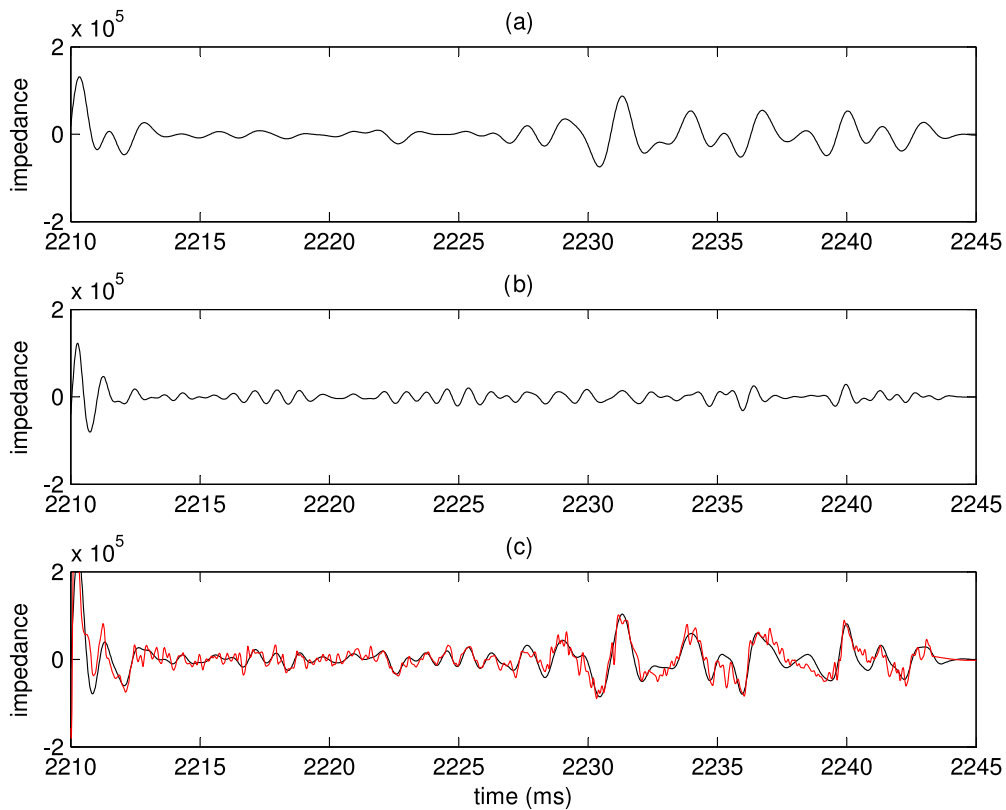
Figure 9. Relative acoustic impedance profiles reconstructed with the inverse wavelet transform applied on the WR of the *in situ* acoustic impedance profile of Fig. 8(a) for (a) the source-corrected WR of the HR component, (b) the source-corrected WR of the VHR component and (c) the source-corrected WR when both the HR and VHR sources are merged (black line) and the reference WR with $a \in \mathbb{R}^+$ (red line, similar to Fig. 8b).

two seismic data sets. But already, we present here what we can get when working with a HR and a VHR seismic data sets, each composed by 450 seismic traces in the vicinity of the *in situ* subseabed samples (Fig. 11). When we process the fusion of both data sets, the reconstruction of the impedance profile is improved as shown in the previous section, that is, the vertical resolution is better than what can be expected with the HR and VHR seismic sources: the subseabed imaging of the impedance profiles is plotted in Fig. 12(a). The strong contrast at $t \simeq 2210$ ms is due the partial reconstruction process of the relative profile which dominates at the seafloor interface. Geological layers can be clearly identified in the subsurface, with a vertical resolution of 38 cm: we are now able to follow and quantify spatial variations of the subseabed acoustic impedance. We remember that we do not have access to the low frequency content of the impedance profile, removed by the integration of the Green's function. But it is interesting to highlight that if the large scale physical properties measured at the core sample location can be extended to the seismic imaging area, the absolute impedance profile can be determined with high confidence. Moreover, we have shown in Ker *et al.* (2011) that the acoustic impedance of the core sample is mainly controlled by density variations, that is, the sound velocity $Vp = 1485 \text{ m s}^{-1}$ is roughly constant. With these realistic assumptions, we are able to propose a quantitative information of the seabed physical properties and we can image the density structure of the subseabed with respect to the depth (Fig. 12b).

Another point to highlight is the low computational cost of the present method to quantify the subseabed structure from the inverse wavelet transform of the source-corrected WR_e (eq. 13). The potential of this approach is obvious in order to get a quick preview

of the subseabed impedance profile but also to process very large seismic data sets.

6 CONCLUSION

The potential of the new wavelet-based developments, which involve the theoretical properties of both the wavelet transform and Lévy-alpha stable functions, is of particular interest when merging multiresolution data from different seismic sources. Actually, we show that fractional derivative orders allow adapting a source model for each seismic source and we are now able to merge such data, an original fusion processing that spans the analysis frequency range required for multiscale seismic imaging of complex subseabeds. Moreover, we develop the source-corrected WR of seismic reflectors with respect to a new parametrization based on the dominant period, or breadth of the wavelet, in accordance with both the wavelet formalism and the temporal resolution of the seismic sources.

Applied on a homogeneous thin layer, we illustrate the efficiency of the method to correct complex reflectors WR performed by merging the high resolution and very high resolution seismic sources of the SYSIF deep-towed device. The corrected ridge functions, proposed as multiscale seismic attributes, are in perfect agreement with the reference ridge functions and the transition between the both contributions does not suffer from discontinuity anymore, allowing working in the continuous dominant dilation range covered by the merged multiresolution seismic sources. We also show the efficiency of the method with complex impedance structures defined from ground truth data where seismic reflectors can be identified: their multiscale seismic attributes are fully corrected over the whole frequency broadband of the SYSIF device.
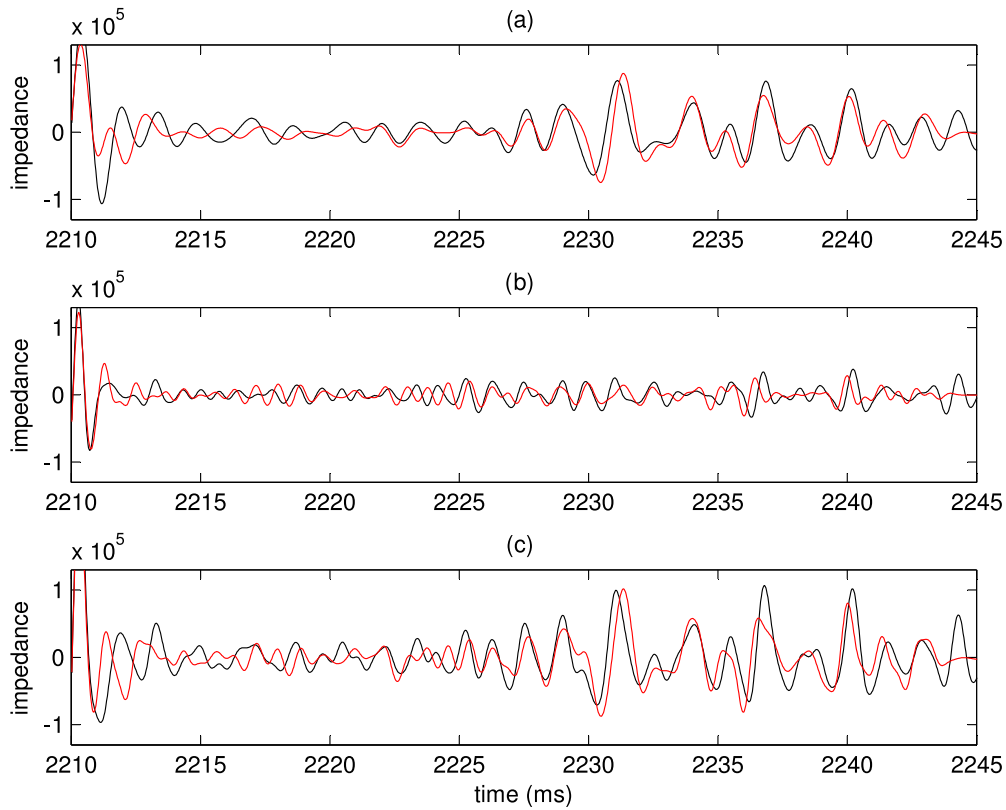
Figure 10. Relative acoustic impedance profiles reconstructed with the inverse wavelet transform applied on the WR of the seismic data (black lines) and *in situ* acoustic impedance profile (in red) for (a) the source-corrected WR of the HR component, (b) the source-corrected WR of the VHR component and (c) the source-corrected WR when both the HR and VHR sources are merged.
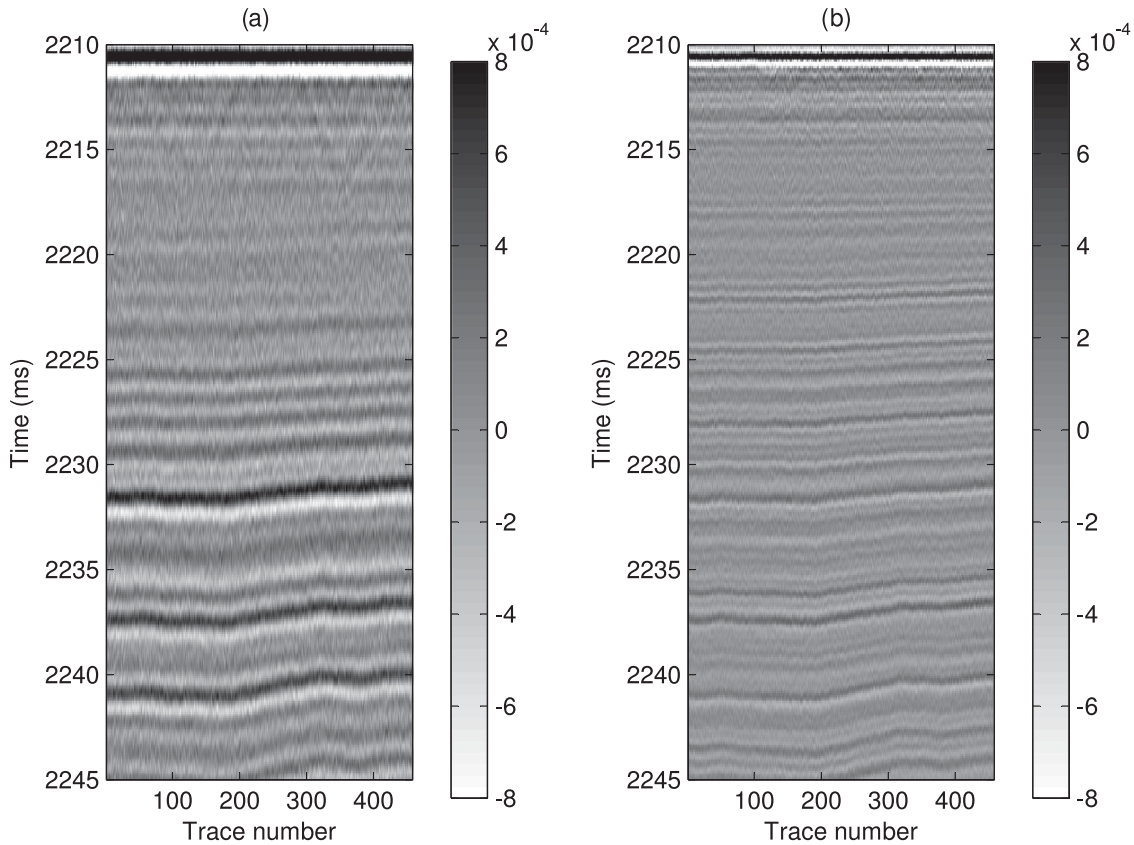
Figure 11. (a) HR seismic profile. (b) VHR seismic profile. The *in situ* impedance profile is located close to trace number 273.
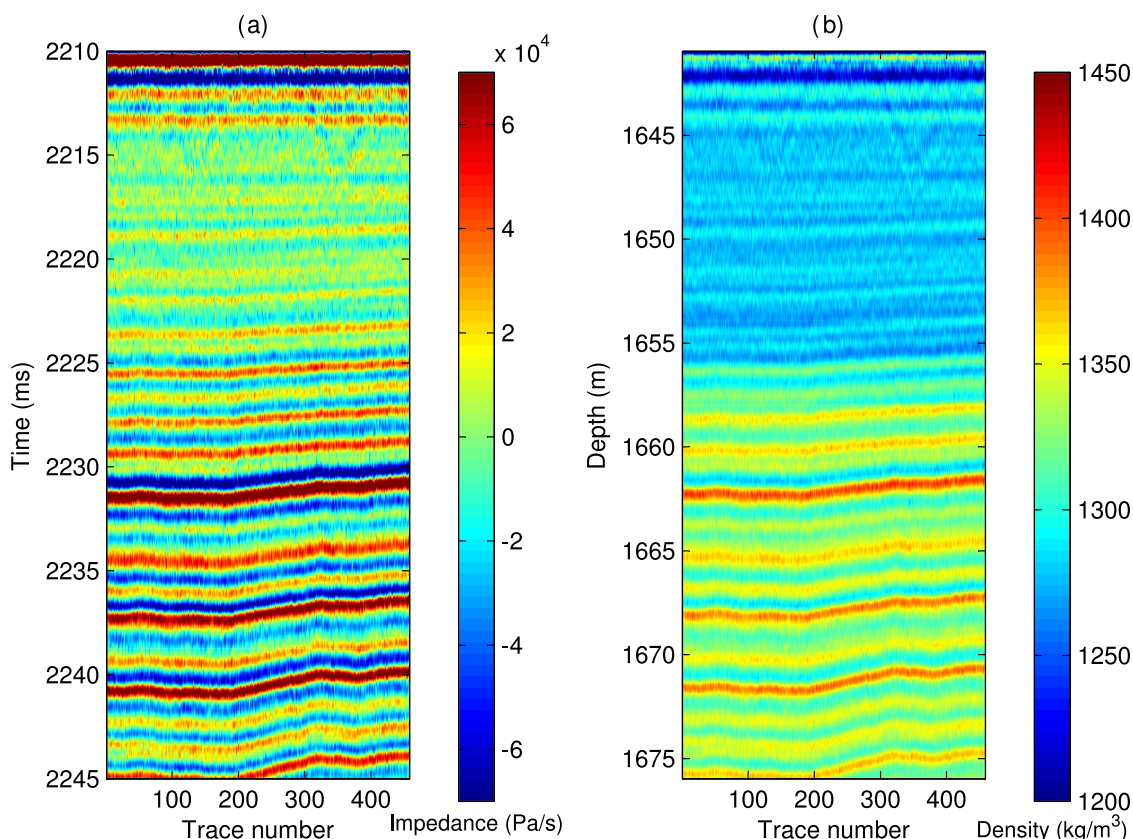
Figure 12. (a) Subseabed imaging of the relative acoustic impedance profiles reconstructed with the inverse wavelet transform of the source-corrected WR of seismic data when both the HR and VHR sources are merged. (b) Associated subseabed density imaging with the assumption of a lateral extension for the low frequency content of the local *in situ* impedance profile.

Thanks to the wavelet-based method to remove the seismic source filtering effects, we also take advantage of the inverse wavelet transform properties extended to the source-corrected WR (Fig. 1). With a first application to reconstruct the acoustic impedance profile of the subseabed, we illustrate that merging both the HR and VHR sources of the SYSIF device allows working with a very broad-band seismic source that improves the vertical resolution of the relative impedance profile. We note that the method benefits from a low computation cost which efficiency can be increased by implementing the simplified reconstruction formula of the inverse wavelet transform (Farge 1992), in particular when assessing physical properties of the subseabed over large seismic data sets. Promising for future works in subseabed geophysical imaging, the source-corrected WR is a powerful method to merge multiresolution seismic sources and can be extended to more general acoustic source signals in the context of multisensor fusion.

REFERENCES

Bracewell, R.N., 1999. *The Fourier Transform and its Applications,* 3d edn, McGraw-Hill Science/Engineering/Math, 640 pp.

Brcich, R.R., Iskander, D.R. & Zoubir, A.M., 2005. The stability test for symmetric alpha-stable distributions, *IEEE Trans. Signal Process.,* **53,** 977–981.

Castagna, J., Sun, S. & Siegfried, R.W., 2003. Instantaneous spectral analysis: detection of low-frequency shadows associated with hydrocarbons, *Leading Edge,* **22,** 120–127.

Chopra, S. & Marfurt, K., 2005. Seismic attributes—a historical perspective, *Geophysics,* **70,** 3SO–28SO.

Dong, J., Zhuang, D., Huang, Y. & Fu, J., 2009. Advances in multi-sensor data fusion: algorithms and applications, *Sensors,* **9,** 7771–7784.

Farge, M., 1992. Wavelet transforms and their applications to turbulence, *Annu. Rev. Fluid Mech.,* **24,** 395–457.

Fomel, S., 2007. Local seismic attributes, *Geophysics,* **72,** A29–A33.

Garguet-Duport, B., Girel, J., Chassery, J.-M. & Pautou, G., 1996. The use of multiresolution analysis and wavelets transform for merging SPOT panchromatic and multispectral image data, *Photogramm. Eng. Remote Sens.,* **62**(9),1057–1066.

Gesret, A., Laigle, M., Diaz, J., Sachpazi, M. & Hirn, A., 2010. The oceanic nature of the African slab subducted under Peloponnesus: thin-layer resolution from multiscale analysis of teleseismic P-to-S converted waves, *Geophys. J. Int.,* **183,** 833–849.

Gutowski, M., Bull, J., Henstock, T., Dix, J., Hogarth, P., Leighton, T. & White, P., 2002. Chirp sub-bottom source signature design and field testing, *Mar. Geophys. Res.,* **23,** 481–492.

Kallweit, R.S. & Wood, L.C., 1982. The limits of resolution of zero-phase wavelets, *Geophysics,* **47,** 1035–1046.

Kilbas, A., Srivastava, H. & Trujillo, J., 2006. *Theory and Applications of Fractional Differential Equations,* Elsevier.

Ker, S., Marsset, B., Garziglia, S., Le Gonidec, Y., Gibert, D., Voisset, M. & Adamy, J., 2010. High-resolution seismic imaging in deep sea from a joint deep-towed/OBH reflection experiment: application to a Mass Transport Complex offshore Nigeria, *Geophys. J. Int.,* **182,** 1524–1542.

Ker, S., Le Gonidec, Y., Gibert, D. & Marsset, B., 2011. Multiscale seismic attributes: a wavelet-based method and its application to high-resolution seismic and ground truth data, *Geophys. J. Int.,* **187,** 1038–1054.

Ker, S., Le Gonidec, Y. & Gibert, D., 2012. Multiscale seismic attributes: source-corrected wavelet response and its application to high-resolution seismic data, *Geophys. J. Int.,* **190,** 1746–1760.

Le Gonidec, Y. & Gibert, D., 2007. Multiscale analysis of waves reflected by granular media: acoustic experiments on glass beads and effective medium theories, *J. geophys. Res.,* **112**(B05103), doi:10.1029/2006JB004518.

Le Gonidec, Y., Gibert, D. & Proust, J.-N., 2002. Multiscale analysis of waves reflected by complex interfaces: basic principles and experiments, *J. geophys. Res.,* **107**(B9), 2184.

Le Gonidec, Y., Conil, F. & Gibert, D., 2003. The wavelet response as a multiscale NDT method, *Ultrasonics,* **41,** 487–497.

Mallat, S., 1998, *A Wavelet Tour of Signal Processing,* 2nd edn, Academic Press.

Mallat, S. & Hwang, W. L., 1992. Singularity detection and processing with wavelets, *IEEE Trans. Inf. Theory,* **38,** 617–643.

Marsset, T., Marsset, B., Ker, S., Thomas, Y. & Le Gall, Y., 2010. High and very high resolution deep-towed seismic system: performance and examples from deepwater Geohazard studies, *Deep-Sea Res. I,* **57,** doi:10.1016/j.dsr.2010.01.001.

Miller, K.S. & Ross, B., 1993. *An Introduction to the Fractional Calculus and Fractional Differential Equations,* John Wiley and Sons.

Moreau, F., Gibert, D., Holschneider, M. & Saracco, G., 1997. Wavelet analysis of potential fields, *Inverse Probl.,* **13,** 165–178.

Moreau, F., Gibert, D., Holschneider, M. & Saracco, G., 1999. Identification of sources of potential fields with the continuous wavelet transform: basic theory, *J. geophys. Res.,* **104,** 5003–5013.

Morlet, J., Arens, G., Forgeau, I. & Giard, D.1982. Wave propagation and sampling theory—part I: complex signal and scattering in multilayered media, *Geophysics,* **47,** 203, doi:10.1190/1.1441328.

Partyka, G., Thomas, J., Turco, K. & Hartmann, D., 2000. Upscaling petrophysical properties to the seismic scale, *in Proceedings of the 70th Annual International Meeting,* Calgary, SEG Expanded Abstracts.

Pennington, W.D., 2001. Reservoir geophysics, *Geophysics,* **66,** 25–30.

Sailhac, P., Gibert, D. & Boukerbout, H., 2009. The theory of the continuous wavelet transform in the interpretation of potential fields: a review, *Geophys. Prospect.,* **57,** 517–525.

Voit, J., 2003. *The Statistical Mechanics of Financial Markets (Texts and Monographs in Physics),* Springer-Verlag.

Widess, M.A., 1973. How thin is a thin bed?, *Geophysics,* **38,** 1176–1180.

Wood, W., Gettrust, J.F. & Spychalski, S., 2003, A new deep-towed, multichannel seismic system, *Sea Technol.,* **44,** 44–49.

Yilmaz, O., 2001, *Seismic Data Processing,* Society of Exploration Geophysicists.

Zhou, J., Civco, D.L. & Silander, J.A., 1998. A wavelet transform method to merge Landsat TM and SPOT panchromatic data, *Int. J. Remote Sens.,* **19,** 743–757.